Journal of Power Sources 231 (2013) 190–196

Contents lists available at SciVerse ScienceDirect

Journal of Power Sources

journal homepage: www.elsevier.com/locate/jpowsour

Kinetics of sodium borohydride hydrolysis catalyzed via carbon nanosheets supported Zr/Co

Xuan Zhang [a], Zhenhua Wei [b,**], Qingjie Guo [a,*], Hongjing Tian [a]

[a] College of Chemical Engineering, Qingdao University of Science and Technology, Qingdao 266042, China
[b] Institute of Oceanology, Chinese Academy of Sciences, Qingdao 266071, China

HIGHLIGHTS

- Peanut shells can be readily converted into porous carbon nanosheets in a fluid bed.
- Zr/Co/C catalyst has been obtained by loading Zr and Co on the carbon surface.
- Zr/Co/C exhibits good catalytic activity for $NaBH_4$ hydrolysis in PEM fuel cells.
- A kinetic rate equation for Zr/Co/C catalyzed hydrolysis of $NaBH_4$ is obtained.

GRAPHICAL ABSTRACT

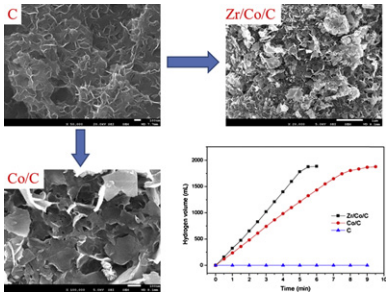

ARTICLE INFO

Article history:
Received 26 September 2012
Received in revised form
25 November 2012
Accepted 1 January 2013
Available online 9 January 2013

Keywords:
Hydrogen
Sodium borohydride
Carbon-supported zirconium/cobalt
Kinetics

ABSTRACT

Porous sheet-like activated carbon was prepared in a fluidized bed using peanut shell as carbon precursor. Cobalt and zirconium were impregnated onto the carbon by impregnation-chemical reduction method to obtain carbon nanosheets supported Co and Zr/Co catalysts. The samples were characterized using field emission scanning electron microscopy, X-ray diffraction, H_2-temperature-programmed reduction, and nitrogen adsorption measurements. It was found that the introduction of zirconium to the carbon-supported cobalt led to an intensified interaction between cobalt and the support. With the activation energy of 34.84 kJ mol^{-1} and maximum hydrogen generation rate of 1708 mL min^{-1} g^{-1}, this novel carbon-supported Zr/Co catalyst exhibited superior catalytic activity for the hydrolysis of $NaBH_4$ in alkaline medium. Furthermore, the effects of temperature, catalyst amount, and concentration of NaOH and $NaBH_4$ on the hydrolysis process were systematically studied, and an overall kinetic rate equation was described as $r = Ae^{-34840/(RT)}[\text{catalyst}]^{1.53}[\text{NaOH}]^{-0.54}[\text{NaBH4}]^{0.43}$.

© 2013 Elsevier B.V. All rights reserved.

1. Introduction

The development of low-cost, eco-friendly, and sustainable energy sources is undoubtedly one of the greatest challenges facing humanity due to increasing concerns over a series of worldwide energy and environmental problems. In the past decades, research around nanoscale interface technologies related to photovoltaics, batteries and fuel cells has brought fascinating breakthroughs in energy conversion and storage [1–3]. In particular, so much attention has been paid to hydrogen fuel cells as attracting clean and efficient power generation devices that they are now on the verge of commercialization in transportation applications [4–6]. However, one of the unsolved problems for mobile applications of hydrogen fuel cells technology is the cost-effective generation and safe storage of hydrogen [7].

Considerable efforts have proved that sodium borohydride ($NaBH_4$) can be a safer alternative than compressed or liquefied

* Corresponding author. Tel.: +86 532 84022506; fax: +86 532 84022757.
** Corresponding author.
E-mail addresses: qj_guo@yahoo.com, geneway@126.com (Q. Guo).

0378-7753/$ – see front matter © 2013 Elsevier B.V. All rights reserved.
http://dx.doi.org/10.1016/j.jpowsour.2013.01.008

hydrogen. $NaBH_4$ exhibits the advantages of high hydrogen storage density, together with an easy hydrogen release through a hydrolysis reaction ($NaBH_4 + 2H_2O \rightarrow NaBO_2 + 4H_2$) that can be controlled catalytically [7–9]. It is worth noticing that this reaction produces pure and slightly humid hydrogen that can be directly used in proton exchange membrane (PEM) fuel cells. Moreover, the only by-product ($NaBO_2$) is environmentally benign and can be recycled back to $NaBH_4$. Because the hydrogen production process of $NaBH_4$ hydrolysis is largely dependent on the catalyst, many efforts have been directed toward design of catalysts less costly and more separable than typically used noble metals such as Pt [10], Ru [11], and Pd [12], and cobalt-based catalysts were found to have high activity and stability [8,9,13,14]. As the major limiting step for the reaction is the accessibility of the active sites, the use of nanomaterials has attracted increasing interest. Besides, supported catalysts are highly promising owning to their advantages of easy separation, reusability, and cost-effectiveness [15–17].

It has been abundantly reported that carbon-supported cobalt can be used as a potential catalyst for the hydrolysis of $NaBH_4$ in alkaline solutions because activated carbon is very stable in strong alkaline solutions and possesses high specific surface area which is helpful for the dispersion of active catalysts [18–20]. However, all the reported carbon supports are commercially available or prepared by pure precursors such as glucose. There is neither report on carbon support directly prepared by cheap biomass waste, nor is there any report on the influence of introducing other metals on the hydrogen production activity of carbon-supported cobalt catalysts. In this report, the abundantly available biomass waste, peanut shell, is used as a precursor to fabricate activated carbon with nanosheet structure, and a novel zirconium-doped carbon-supported cobalt catalyst is prepared by impregnation-chemical reduction method using the carbon nanosheets as support. The catalytic performance of the catalyst for the hydrolysis of $NaBH_4$ in alkaline media is also systematically investigated and evaluated.

2. Experimental

2.1. Preparation of carbon nanosheets

Raw peanut shells for the preparation of activated carbon nanosheets were collected from local market in Qingdao, China. Peanut shells were first washed and dried at 100 °C overnight and then ground and sieved to 200 mesh (74 μm). After that, the biomass particles were placed into a fluidized bed under a stream of N_2. The fluidized bed was heated at a rate of 25 °C min^{-1} to 500 °C with a 1 h hold at this temperature, then, it was further heated to 800 °C while the atmosphere was switched to CO_2. The carbonized peanut shell particles were then activated under CO_2 at 800 °C for 2 h. After that, the sample was treated with 30% HNO_3 solution at 60 °C for 5 h, and then it was rinsed thoroughly with distilled water to remove minerals and ash before dried at 60 °C for use.

2.2. Preparation of the catalysts

The catalysts were prepared by impregnation-chemical reduction method. Typically, a required amount of cobalt nitrite ($Co(NO_3)_2{\cdot}6H_2O$) and zirconium nitrate ($Zr(NO_3)_4{\cdot}5H_2O$) was dissolved in 50 mL of distilled water. Then, 5 g of the as-prepared activated carbon was added into this solution and the mixture was treated under ultrasound with a frequency of 60 kHz for 30 min. The excess of water was evaporated at 120 °C for 10 h and the Co and Zr precursors were reduced by means of 2.65 M $NaBH_4$ solution. After that, the mixture was filtered, rinsed, and dried in a vacuum. Finally, the sample was calcined in a N_2 flow at 450 °C for 4 h to obtain the carbon-supported Zr/Co catalyst (denoted as Zr/Co/C) with 5 wt% of Zr. The carbon-supported Co catalyst (denoted as Co/C) with 10 wt% of Co was obtained in the same way, except that $Zr(NO_3)_4{\cdot}5H_2O$ was not added in the process.

2.3. Characterization

The morphology of the as-prepared activated carbon and the catalysts were examined with a JEOL JSM-6700F field emission scanning electron microscope (FESEM) equipped with energy dispersive X-ray spectroscopy (EDS). Powder X-ray diffraction (XRD) patterns of the samples were obtained with a D8 Advance X-ray diffractometer at 40 kV and 100 mA using monochromatic Cu Kα radiation. After solubilization of the samples in H_2SO_4:HNO_3:HCl solutions, elemental analysis was performed using a Thermo-Fisher inductively coupled plasma optical emission spectrometer (ICP-OES). The specific surface area, total pore volume, and average pore size of the samples were measured by nitrogen physisorption using a Quantachrome Autosorb-1C system after the samples had been degassed under a flow of N_2 at 180 °C for 6 h. The surface area was estimated by the Brunauer–Emmett–Teller (BET) method, and the average pore size and total pore volume were determined by the Barrett–Joyner–Halenda (BJH) method. Temperature-programmed reduction (TPR) experiments were conducted under a mixed atmosphere of 8 vol% of H_2 in N_2 with a total flow rate of 45 mL min^{-1}, while the temperature was increased to 800 °C at a heating rate of 5 °C min^{-1}. The H_2 consumption rate was monitored in a thermal conductivity detector (TCD) calibrated previously using the reduction of CuO as the standard.

2.4. Catalytic activity experiments

All the hydrogen generation experiments were initiated by dropping a desired amount of catalyst into the $NaBH_4$–NaOH solution in a flask quickly. The flask was under water bath to maintain at a given temperature. During the reaction process, a wet gas meter was used to measure the cumulative volume of the generated hydrogen over time. No further stirring was adopted during the reaction because the produced hydrogen can generate vigorous bubble in the reactor hence facilitate the contact between the reactant and the catalyst.

It is commonly known that the hydrolysis rate of $NaBH_4$ depends on factors such as solution temperature, amount of catalyst, and concentration of $NaBH_4$ and NaOH [11,20,21]. Therefore, we carried out a series of experiments to examine the effects of these factors on hydrogen production. Hydrogen generation rate was measured at different temperatures (25, 30, 35, 40 °C) to determine the activation energy, and different dosages or concentrations of the catalyst (0.05–0.2 g), NaOH (1–10 wt%) and $NaBH_4$ (1–15 wt%) were used for the measurements in which one parameter was varied while the others were kept constant.

3. Results and discussion

3.1. Characterization

The surface area and pore size distribution of the as-prepared activated carbon were determined with nitrogen adsorption–desorption measurements. Fig. 1 shows a typical IV isotherm with a steep adsorption rise below the relative pressure of 0.1 and a hysteresis loop in the relative pressure range of 0.5–0.95, indicating that the as-prepared activated carbon possessed microporous and mesoporous structures. The BET surface area and the total pore volume of the sample were calculated to be as high as 1059 m^2 g^{-1} and 0.8 cm^3 g^{-1}, respectively. In addition, the BJH pore size distribution (inset of Fig. 1) obtained from the isotherm

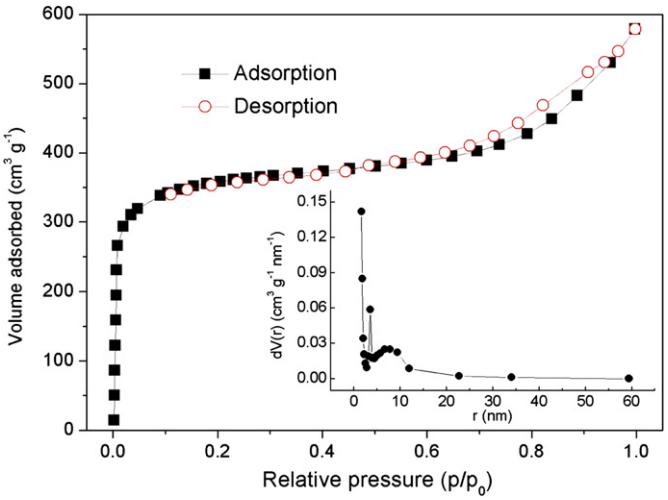

Fig. 1. N_2 adsorption–desorption isotherm (inset: pore size distribution) of the as-prepared activated carbon.

suggests that the sample contained narrowly distributed pores with sizes generally below 20 nm.

Porous activated carbons with high specific area are commonly employed for catalyst supports because their superior capability to adsorb, stabilize, and disperse the active catalysts [10,17]. Inspired by this idea, we investigated the application of the as-prepared peanut based carbon as support for cobalt and zirconium oxides. Fig. 2 shows the morphology of the as-prepared carbon support, the Co/C and Zr/Co/C catalysts. The porous nanosheet nature of the peanut shell based carbon is clearly revealed in Fig. 2a and b, where petal-like sheets with thickness of less than 10 nm interconnected with each other, forming well-defined porous structure. The Co/C (Fig. 2c) and Zr/Co/C (Fig. 2d) catalysts also exhibited nanosheet structures, which contained many broken and irregular particles on the surfaces, especially for Zr/Co/C. It has been reported that the carbonization and acidification treatment of biomass can result in lots of surface oxygen-containing functional groups which form anchoring sites for metallic precursors [18]. Thus, it is quite conceivable here that these oxygen-containing groups played an major role in binding or coordinating cobalt and zirconium ions onto the surface of the carbon nanosheets, leading to the formation of dispersive Co_3O_4 and ZrO_2.

The chemical composition and phase purity of the samples were determined by XRD, which confirms that Co_3O_4 and ZrO_2 were successfully loaded on the carbon nanosheets support, as shown in Fig. 3. It is evident that the main diffraction peaks located at 33.3°, 36.9°, 45.1°, 59.4°, and 65.4° in the XRD pattern of the Co/C sample can be well assigned to Co_3O_4, which is in good agreement with previous findings where Co_3O_4 was also obtained with calcination after impregnation [22]. Furthermore, the pattern of the Zr/Co/C sample appears some main characteristic peaks of ZrO_2 located at 31.8°, 50.6°, and 60.9°, indicating the formation of crystalline ZrO_2. The diffraction peaks of Co_3O_4 in Zr/Co/C were sharper and narrower than that in Co/C, which suggests an increase in the crystalline size of Co_3O_4 with the introduction of zirconium in the catalyst. According to the full width at the half-maximum of the diffraction peaks, the average crystallite size (estimated by the Scherrer equation) of Co_3O_4 in Co/C and Zr/Co/C was 33.7 and 67.1 nm, respectively.

EDS and ICP-OES were further used to determine the loading content of Co and Zr on the carbon nanosheets of the two catalysts. As shown in Table 1, the values obtained using both EDS and ICP-OES were very close to the theoretical loadings. It is interesting to note that some deviations were observed between the two methods of analysis. EDS is typically a quick and simple method for characterization of carbon based catalysts, and with proper sample preparation and adequate data capture it can produce reliable results [9]. It is believed the deviations here are attributed to the

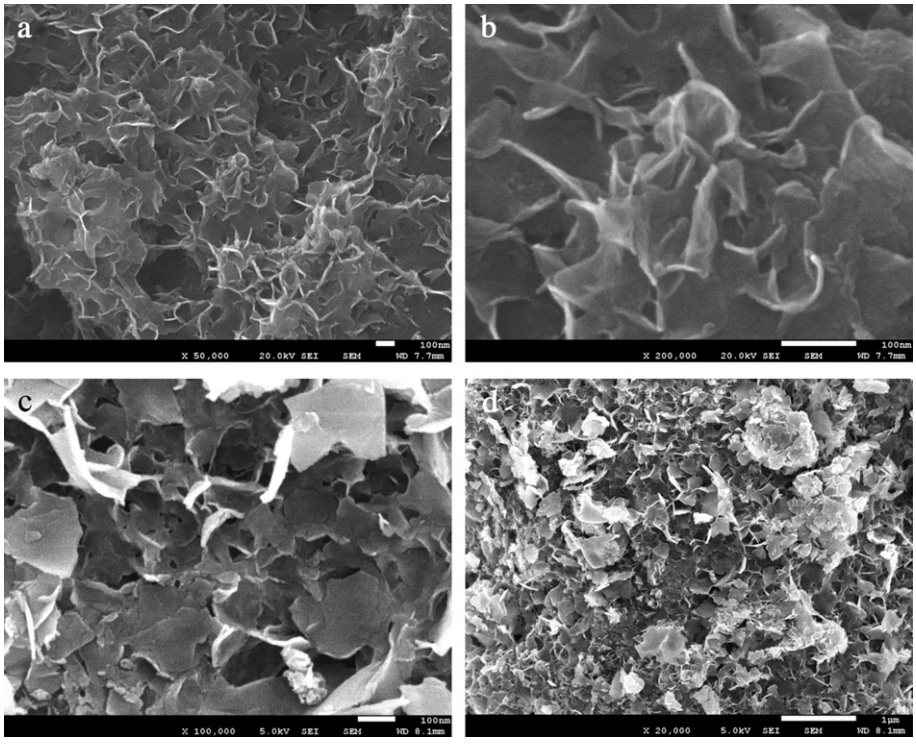

Fig. 2. FESEM images of the carbon nanosheets (a, b), the Co/C (c) and the Zr/Co/C (d) catalysts.

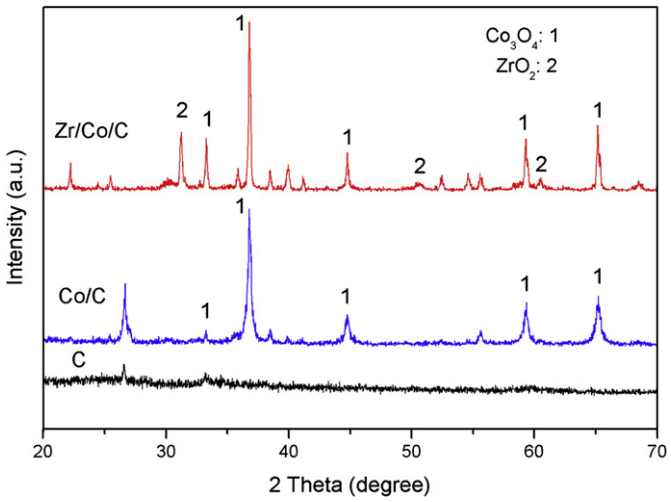

Fig. 3. XRD patterns of the carbon nanosheets, the Co/C, and the Zr/Co/C catalysts.

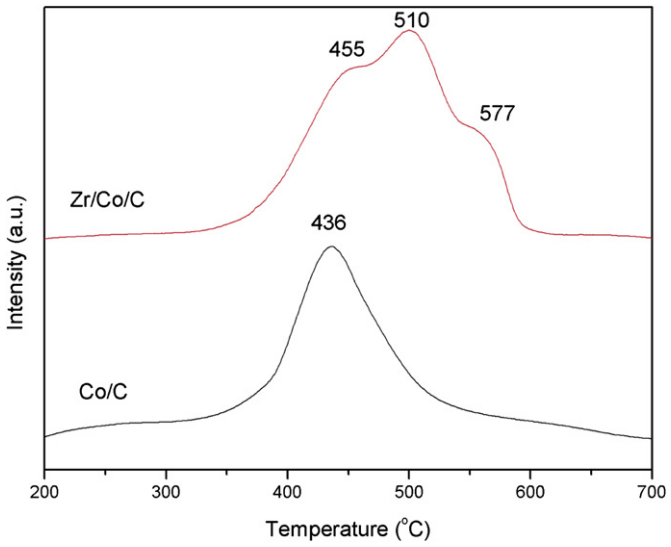

Fig. 4. TPR profiles of the Co/C and Zr/Co/C catalysts.

small sample size used for the EDS analysis. However, the values obtained by EDS analysis were not so much deviated from those determined by ICP analysis reflecting the overall metal content of a relatively large amount of sample, which in turn, demonstrates a good distribution and dispersion of Co_3O_4 and ZrO_2 on the carbon support.

As a useful way to obtain information about the degree of interaction of the supported phase with the carrier [23], TPR was performed to determine the reduction behaviors of Co_3O_4 and ZrO_2 in the catalysts, as shown in Fig. 4. For the Co/C catalyst, there appears only one reduction peak at the temperature of 436 °C, which is different from the double peaks for Co_3O_4 reported previously [22,24]. This difference was likely due to the porous carbon nanosheets support with a large surface area, which resulted in fine dispersion of nanosized Co_3O_4 nanoparticles. Hence, Co_3O_4 could fully contact with the reduction atmosphere and the typically observed two-step reduction ($Co^{3+} \rightarrow Co^{2+} \rightarrow Co^0$) was perfectly overlapped. For the Zr/Co/C catalyst, the introduction of ZrO_2 markedly affected the reduction behavior of the catalyst. On one hand, a broad triplet peak was observed in the temperature range of 350–600 °C, suggesting an interaction between surface Co_3O_4 species and the doped ZrO_2. The first two protuberances at 455 and 510 °C attributed to the two-step reduction of Co_3O_4 shifted to a higher temperature, indicating a stronger interaction between cobalt and the carbon support. On the other hand, the ZrO_2 reduction was shown by a protuberance at 577 °C, a temperature a little higher than that for the reduction of pure ZrO_2, which was likely due to the reduction of Co_3O_4–ZrO_2 interaction species [22]. These results indicate that the addition of ZrO_2 led to an intensified interaction between the components in the Zr/Co/C catalyst.

3.2. Performance of the catalysts

The catalytic test of the two catalysts for $NaBH_4$ hydrolysis was carried out. The reaction solution was 15 mL of 5 wt% $NaBH_4$ and 2 wt% NaOH, and the amount of the catalysts was 0.2 g. The hydrolysis reaction was also performed in the presence of the bare carbon nanosheets support in order to understand if the support could act as catalyst due to its porous composite nature. As highlighted in Fig. 5, obviously, the carbon support had no catalytic activity toward the hydrolysis of $NaBH_4$. In contrast, both Co/C and Zr/Co/C exhibited notably fast hydrogen generation kinetics, which indicates that the active components of the catalysts were Co_3O_4 and ZrO_2 rather than the carbon support. Moreover, the reaction using the Zr/Co/C catalyst completed within a much shorter time than that using the Co/C catalyst, suggesting that the addition of ZrO_2 in the catalyst had a significant effect on the rate of $NaBH_4$ hydrolysis. Table 2 also shows that the maximum hydrogen generation rate of Zr/Co/C was much higher than those of most of previous cobalt-based catalysts. We believe such an enhanced hydrogen generation rate is related to the increased crystallite size of Co_3O_4 and the intensified interaction between cobalt and the support in the presence of zirconia, as confirmed by the above-mentioned characterization analysis. Since Zr/Co/C exhibited

Table 1
The loading content of Co and Zr on Co/C and Zr/Co/C.

Catalyst	Theoretical content (wt%)		Content from EDS (wt%)		Content from ICP-OES (wt%)	
	Co	Zr	Co	Zr	Co	Zr
Co/C	10	–	9.7	–	9.4	–
Zr/Co/C	10	5	9.3	4.1	9.5	4.5

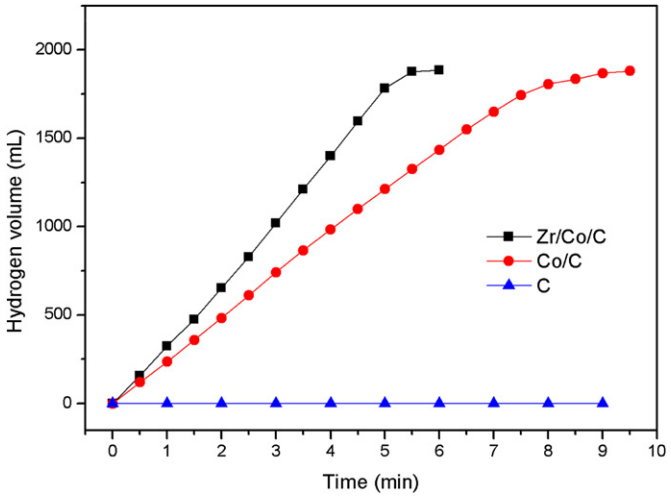

Fig. 5. The hydrogen generation performance of the carbon nanosheets, the Co/C, and the Zr/Co/C catalysts.

Table 2
Hydrogen generation rate and activation energy of various cobalt-based catalysts.

Catalyst	Preparation method	Hydrogen generation rate (mL min^{-1} g^{-1})	Activated energy (kJ mol^{-1})	Reference
Co–B	Chemical reduction	875	64.87	[25]
Ni–Co–B	Chemical reduction	168	62.00	[26]
Multiwalled carbon nanotubes supported Co	Impregnation-chemical reduction	5100	40.40	[27]
Carbon-supported Co–B	Impregnation-chemical reduction	1268	57.80	[28]
Activated carbon-supported Co	Impregnation-chemical reduction	–	45.64	[29]
γ-Al_2O_3 supported Co catalyst	Impregnation-chemical reduction	220	32.63	[29]
Ni-foam supported Co–B	Modified electroless plating	663	33.00	[30]
Attapulgite clay-supported Co–B	Impregnation-chemical reduction	1271	56.32	[31]
Carbon nanosheets supported Zr/Co	Impregnation-chemical reduction	1708	34.84	This work

better catalytic activity than Co/C, it was chosen as the research focus in the following experiments.

3.3. Kinetic experiments

It is of great significance to investigate the kinetics of $NaBH_4$ hydrolysis reaction since it can provide useful information about the role of many experimental factors on the hydrogen generation rate [21]. During the $NaBH_4$ hydrolysis, solution temperature, amount of catalyst, concentration of NaOH and $NaBH_4$ determine the reaction rate, and the hydrogen generation rate equation can be expressed as

$$r = Ae^{-E_a/(RT)}[\text{catalyst}]^x[\text{NaOH}]^y[\text{NaBH}_4]^z \quad (1)$$

where r is the hydrogen generation rate, A the pre-exponential factor, E_a the activation energy, R the universal gas constant, T the hydrolysis temperature, and x, y, z are the reaction orders with respect to the amount of catalyst, the concentration of NaOH and $NaBH_4$, respectively.

3.3.1. Effect of solution temperature

The effect of temperature on the $NaBH_4$ hydrolysis was investigated at a temperature range of 25–40 °C with 0.2 g of Zr/Co/C in 15 mL of 5 wt% $NaBH_4$–2% wt% NaOH. As illustrated in Fig. 6a, the

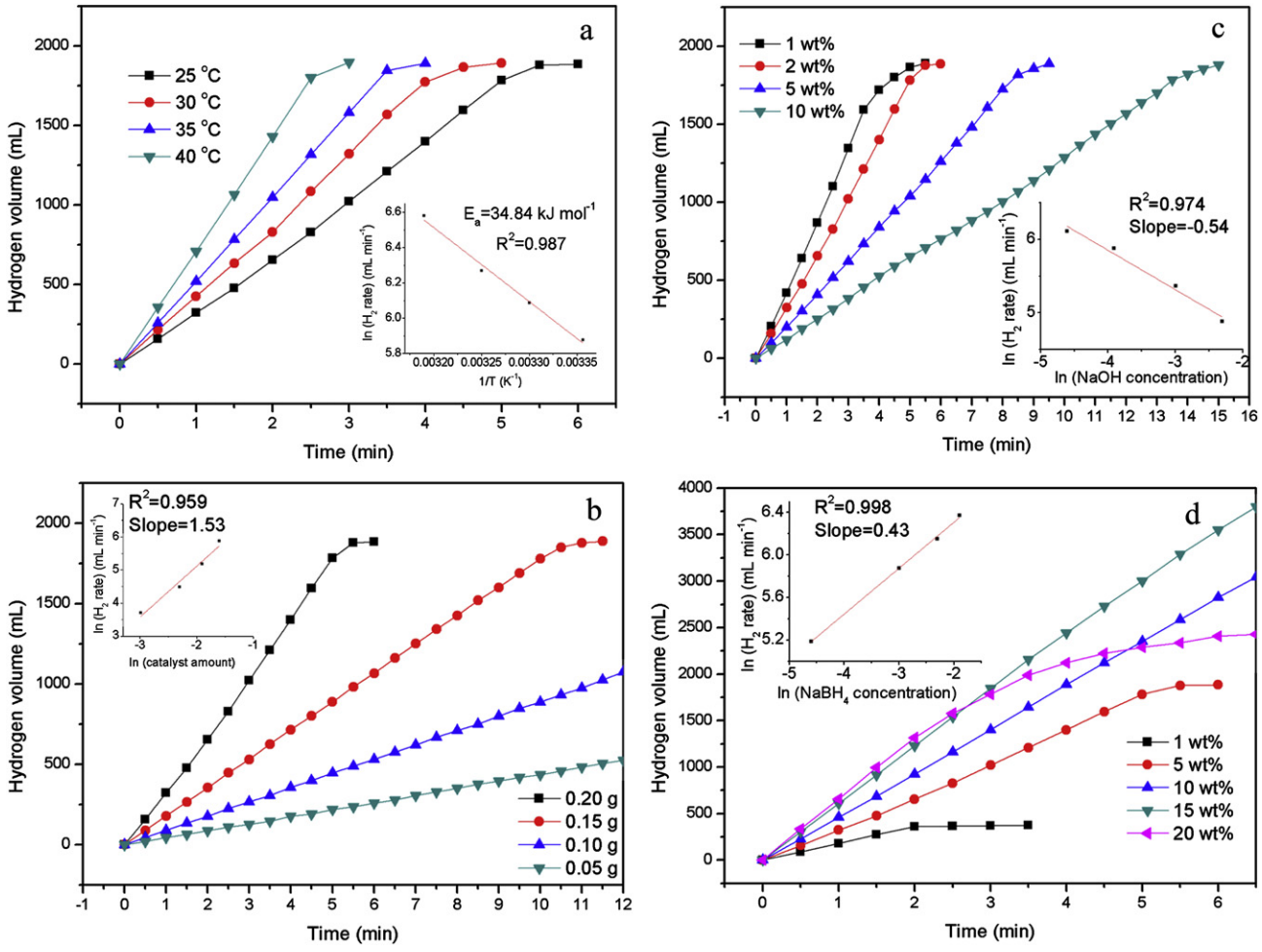

Fig. 6. Effects of temperature (a), amount of catalyst (b), NaOH concentration (c), and $NaBH_4$ concentration (d) on $NaBH_4$ hydrolysis using the Zr/Co/C catalyst.

hydrogen generation rate increased gradually with the solution temperature increasing from 25 to 40 °C. According to the inset Arrhenius plot of ln (r) versus 1/T, the slope of the straight line representing the activation energy was calculated to be 34.84 kJ mol^{-1}. This was a much lower value than those the majority of previously reported cobalt-based catalysts had shown, as listed in Table 2. The favorable activation energy, together with the high catalytic activity and low cost of Zr/Co/C makes it a very promising catalyst in developing PEM fuel cells.

3.3.2. Effect of Zr/Co/C amount

The effect of the Zr/Co/C amount on hydrogen generation rate was investigated by hydrolysis of 15 mL 5 wt% NaBH4–2% wt% NaOH solution at 25 °C varying the amount of Zr/Co/C while keeping other factors constant, and the result is shown in Fig. 6b. Since the hydrogen production process took longer when the catalyst dosages were 0.10 and 0.05 g, only the initial experimental data were selected to draw the figure for these two cases. With the amount of the catalyst increasing from 0.05 to 0.2 g, the average hydrogen generation rate increased gradually from 40.5 to 131.6, 177.7, and 356.4 mL min^{-1}. Hence, the hydrogen generation rate can be controlled by adjusting the catalyst amount used in the hydrolysis reaction. In addition, the ln (r) versus ln (catalyst amount) is plotted in the inset of Fig. 6b, from which we can see the ln (r) changed almost linearly with the ln (catalyst amount), and the slope of the straight line, which determined the order of reaction (x), was 1.53.

3.3.3. Effect of NaOH concentration

The $NaBH_4$ solution can hydrolyze spontaneously when the pH value of the solution is lower than 9. To keep the $NaBH_4$ solution stable at room temperature, NaOH is usually added to the solution as a stabilizer. Nevertheless, the concentration of NaOH significantly affects the hydrogen generation rate. As shown in Fig. 6c, when NaOH concentration varied from 1 wt% to 10 wt% in the presence of 5 wt% $NaBH_4$ solution and 0.2 g of Zr/Co/C at 25 °C, the hydrogen generation rate decreased gradually with increasing NaOH concentrations. At low NaOH concentration of 1 wt%, the reaction rate was quite fast, and the hydrogen production process completed within 6.5 min. When the NaOH concentration increased to 10 wt%, the hydrogen production rate reduced drastically, extending the whole reaction process to 15 min, more than twice as much time as when 1 wt% NaOH was used. The ln (r) versus ln (NaOH concentration) in the inset of Fig. 6c shows that the slope of the straight line was −0.54, confirming NaOH had a negative effect on the hydrogen generation rate. It is worth noting that these findings are different from our previous study where attapulgite clay-supported Co–B was used as the catalyst [31]. In that case, the hydrogen generation rate increased remarkably with increasing NaOH concentrations because high NaOH concentration could promote the production of active Co–B component, which significantly accelerated the hydrolysis. For the Zr/Co/C catalyst in this study, higher concentrations of NaOH would likely lead to reduced activity of water. Meanwhile, the increase of NaOH concentration brings about augmented dense of OH^-, which is considered to be a competitive absorbate of BH_4^- for the catalyst surface [32]. Consequently, more OH^- would occupy the adsorption sites, and it is less likely for BH_4^- to contact with the active components on the Zr/Co/C catalyst, which decreases the hydrogen generation rate.

3.3.4. Effect of $NaBH_4$ concentration

As $NaBH_4$ is the hydrogen source in the hydrolysis reaction, its concentration is the crucial factor that determines the kinetics of the reaction. Therefore, the effect of $NaBH_4$ concentration on the hydrogen generation rate was further studied using $NaBH_4$ with different concentrations (1, 5, 10, 15, and 20 wt%) and 2 wt% NaOH at 25 °C. Fig. 6d shows the hydrogen generation volume as a function of time with the catalyst dosage of 0.2 g. The hydrogen generation rate increased significantly when the concentration of $NaBH_4$ increased from 1 wt% to 15 wt%. However, with the $NaBH_4$ concentration further increased to 20 wt%, the hydrogen generation rate dropped remarkably. Also, unlike most previous reports, the data showed a parabolic tread rather than a linear one even from the beginning of the reaction when 20 wt% $NaBH_4$ was used. A similar observation was made by Xu et al. on carbon-supported cobalt catalyst [19]. They indicated that the decreased hydrogen generation rate may be due to mass transportation limitations resulted from an increased viscosity of the reaction solution.

Here, we believe that mass and heat transfer process should be considered simultaneously when the Zr/Co/C catalyst is studied in the $NaBH_4$ hydrolysis reaction. It is possible that the hydrogen generation rate depends on the competition between the effects of mass transfer and heat transfer. Table 3 lists the viscosity of different concentrations of $NaBH_4$ solution before and after reaction. When the concentration of $NaBH_4$ was below 20 wt%, the solution viscosity obtained was relatively low, and the mass transfer limitation was relatively weak, so the hydrogen generation rate was mainly controlled by heat transfer. As the $NaBH_4$ hydrolysis reaction is exothermic, the higher the $NaBH_4$ concentration is, the more heat will be produced by the hydrolysis reaction. The heat inside the reaction system leads to the increase of reaction temperature, which accelerates the hydrogen generation rate by fast hydrolysis of $NaBH_4$ in the system. However, when the concentration of $NaBH_4$ increases to 20 wt%, the concentration of the produced $NaBO_2$ would also rise remarkably, which gives rise to the increase of the solution viscosity. As calculated from Table 3, with a $NaBH_4$ concentration of 20 wt%, the viscosity of the solution increased by 2707% after the reaction completed, far more than that with $NaBH_4$ concentrations of 1–15 wt%. The increase of viscosity not only limits the mass transfer of $NaBH_4$ from the solution to the inner surface of the catalyst, but also hampers the diffusion of $NaBO_2$ from the catalyst to the reaction solution. As a result, the hydrogen generation rate is predominantly controlled by mass transfer rather than heat transfer, and a relatively low hydrogen generation rate is consequently obtained. In addition, the control experiment reveals that even under mechanical stirring condition of 200 r min^{-1}, the viscosity of the solution with 20 wt% $NaBH_4$ was still quite high when the reaction completed, and the hydrogen generation rate did not change significantly. Hence, only the $NaBH_4$ concentrations less than 20 wt% were adopted to determine the reaction order in the inset of Fig. 6d, where the slope was 0.43.

According to the above investigations, the activation energy and the x, y and z factors for the $NaBH_4$ hydrolysis reaction are obtained, and the final overall kinetic equation with the concentration of $NaBH_4$ less than 20 wt% can be expressed as

$$r = Ae^{-34840/(RT)}[\text{catalyst}]^{1.53}[\text{NaOH}]^{-0.54}[\text{NaBH}_4]^{0.43} \quad (2)$$

Such a quantitative kinetic expression will definitely provide helpful information when the Zr/Co/C catalyst is used for developing PEM fuel cells.

Table 3
Viscosity of different concentrations of $NaBH_4$ solution before and after reaction.

$NaBH_4$ concentration (wt%)	Before reaction (mPa s)	After reaction (mPa s)
1	1.12	1.16
5	1.25	2.34
10	1.31	3.88
15	1.35	6.25
20	1.42	39.86

4. Conclusions

In summary, a novel porous sheet-like activated carbon has been prepared in a fluidized bed using cheap and renewable peanut shell as carbon precursor, and cobalt and zirconium have been successfully impregnated on the carbon nanosheets support by the impregnation-chemical reduction method. The as-prepared Zr/Co/C catalyst shows superior catalytic activity for the hydrolysis of $NaBH_4$. Besides, the overall kinetics of the $NaBH_4$ hydrolysis reaction catalyzed by Zr/Co/C is obtained by a series of experiments. We believe Zr/Co/C has the potential to be used as a cost-effective and sustainable catalyst for the hydrolysis of $NaBH_4$ in PEM fuel cells.

Acknowledgment

The financial support from Natural Science Funds for Distinguished Young Scholar in Shandong Province (JQ200904) and Shandong Province Science & Technology Projects (2009GG10007001) is greatly appreciated.

References

[1] J. Wang, X.B. Zhang, Z.L. Wang, L.M. Wang, Y. Zhang, Energy Environ. Sci. 5 (2012) 6885–6888.
[2] S. Proch, J. Herrmannsdorfer, R. Kempe, C. Kern, A. Jess, L. Seyfarth, J. Senker, Chem. Eur. J. 14 (2008) 8204–8212.
[3] S.S. Muir, X.D. Yao, Int. J. Hydrogen Energy 36 (2011) 5983–5997.
[4] P.K. Cheekatamarla, C.M. Finnerty, J. Power Sourc. 160 (2006) 490–499.
[5] A.F. Ghenciu, Curr. Opin. Solid State Mater. Sci. 6 (2002) 389–399.
[6] S.F. Yin, B.Q. Xu, X.P. Zhou, C.T. Au, Appl. Catal. A Gen. 277 (2004) 1–9.
[7] B.H. Liu, Z.P. Li, J. Power Sourc. 187 (2009) 527–534.
[8] Ö. Metin, S. Özkar, Energy Fuels 23 (2009) 3517–3526.
[9] S. Bennici, H. Yu, E. Obeid, A. Auroux, Int. J. Hydrogen Energy 36 (2011) 7431–7442.
[10] A.C.C. Chang, R.F. Louh, D. Wong, J. Tseng, Y.S. Lee, Int. J. Hydrogen Energy 36 (2011) 8794–8799.
[11] Y.C. Zou, M. Nie, Y.M. Huang, J.Q. Wang, H.L. Liu, Int. J. Hydrogen Energy 36 (2011) 12343–12351.
[12] N. Patel, B. Patton, C. Zanchetta, R. Fernandes, G. Guella, A. Kale, A. Miotello, Int. J. Hydrogen Energy 33 (2008) 287–292.
[13] O. Akdim, R. Chamoun, U.B. Demirci, Y. Zaatar, A. Khoury, P. Miele, Int. J. Hydrogen Energy 36 (2011) 14527–14533.
[14] Q. Li, H. Kim, Fuel Process. Technol. 100 (2012) 43–48.
[15] M. Rakap, S. Özkar, Appl. Catal. B Environ. 91 (2009) 21–29.
[16] M. Rakap, S. Özkar, Catal. Today 183 (2012) 17–25.
[17] A. Doner, I. Karci, G. Kardas, Int. J. Hydrogen Energy 37 (2012) 9470–9476.
[18] D. Xu, P. Dai, Q. Guo, X. Yue, Int. J. Hydrogen Energy 33 (2008) 7371–7377.
[19] D. Xu, P. Dai, X. Liu, C. Cao, Q. Guo, J. Power Sourc. 182 (2008) 616–620.
[20] J. Zhu, R. Li, W. Niu, Y. Wu, X. Gou, J. Power Sourc. 211 (2012) 33–39.
[21] R. Retnamma, A.Q. Novais, C.M. Rangel, Int. J. Hydrogen Energy 36 (2011) 9772–9790.
[22] S. Mu, D. Li, B. Hou, L. Jia, J. Chen, Y. Sun, Energy Fuels 24 (2010) 3715–3718.
[23] Y. Ji, Z. Zhao, A. Duan, G. Jiang, J. Liu, J. Phys. Chem. C 113 (2009) 7186–7199.
[24] Y. Yang, L. Jia, Y. Meng, B. Hou, D. Li, Y. Sun, Catal. Lett. 142 (2011) 195–204.
[25] S.U. Jeong, R.K. Kim, E.A. Cho, H.J. Kim, S.W. Nam, I.H. Oh, S.A. Hong, S.H. Kim, J. Power Sourc. 144 (2005) 129–134.
[26] J.C. Ingersoll, N. Mani, J.C. Thenmozhiyal, A. Muthaiah, J. Power Sourc. 173 (2007) 450–457.
[27] Y. Huang, Y. Wang, R. Zhao, P. Shen, Z. Wei, Int. J. Hydrogen Energy 33 (2008) 7110–7115.
[28] J. Zhao, H. Ma, J. Chen, Int. J. Hydrogen Energy 32 (2007) 4711–4716.
[29] W. Ye, H. Zhang, D. Xu, L. Ma, B. Yi, J. Power Sourc. 164 (2007) 544–548.
[30] H.-B. Dai, Y. Liang, P. Wang, H.-M. Cheng, J. Power Sourc. 177 (2008) 17–23.
[31] H. Tian, Q. Guo, D. Xu, J. Power Sourc. 195 (2010) 2136–2142.
[32] C.-H. Liu, B.-H. Chen, C.-L. Hsueh, J.-R. Ku, F. Tsau, K.-J. Hwang, Appl. Catal. B Environ. 91 (2009) 368–379.